Czech Technical University in Prague
Faculty of Nuclear Sciences and Physical Engineering
Departement of Physics

Field: Experimental Nuclear and Particle Physics

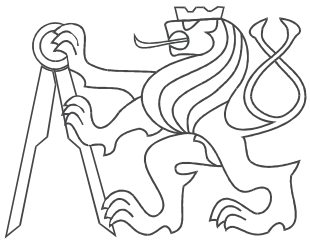

Invisible Energy in Cosmic Ray Showers

RESEARCH PROJECT

Author: Bc. Šimon Novák
Supervisor: RNDr. Petr Trávníček, Ph.D.
Year: 2017

Title: **Invisible Energy in Cosmic Ray Showers**
Author: Bc. Šimon Novák
Field: Experimental Nuclear and Particle Physics
Thesis: Research project
Supervisor: RNDr. Petr Trávníček, Ph.D.
Fyzikální ústav AV ČR, v.v.i.
Consultant: Ing. Jakub Vícha, Ph.D.
Fyzikální ústav AV ČR, v.v.i.
Abstrakt: Ultra high-energy cosmic ray showers created by interactions of cosmic ray particles with the Earth's atmosphere at centre of mass energy exceeding 10^{15} eV are being detected at the Pierre Auger Observatory - the world's biggest experimental site for observation of cosmic rays. For determination of cosmic ray properties a precise measurement of shower energy is required, however the calorimetric energy of a shower measured by fluorescence detectors at the observatory does not represent the absolute shower energy value. A part of the shower energy is carried away by muons and neutrinos and need to be determined from simulated data. A method currently used in shower reconstruction process and also more precise method using measurement of shower muons are studied using simulated data and compared.
Key Words: Pierre Auger Observatory, ultra high-energy cosmic rays, extensive air showers, shower missing energy, muons

Contents

Introduction

The phenomenon of Extensive Air Showers (EAS) as a consequence of a high energy cosmic ray particle hitting Earth's atmosphere is being thoroughly studied for many years since its discovery by physicists Pierre Auger and Walther Bothe in 1930s. Primary particles with energies reaching even 10^{20} eV interact hadronically with atmospheric molecules resulting into creation of many energetic hadrons further interacting with atmosphere. More than 10^{10} new particles emerges through this hadronic and electromagnetic multiplication cascades. Inspected shower parameters such as the depth of electromagnetic or muonic maxima can provide insight into the primary particle composition and its energy. These shower studies are considered to possibly clarify primary cosmic rays origins as well as to improve hadronic interaction models at high energies.

Currently several surface detector experiments are operated in both hemispheres. Some of the most important are the Telescope Array in Utah and the largest cosmic ray detector array - the Pierre Auger Observatory (PAO) in Argentina [1]. Hybrid detector approach with cooperation of surface detectors and fluorescence detectors is used in both observatories and enables to collect more precise cosmic ray data every year. Both observatories are also in progress of augmentation and enhancement of measuring devices - The AugerPrime upgrade at the Pierre Auger Observatory or the TALE extension at the Telescope Array.

This research project aims to understand the process of shower reconstruction at the PAO such as the energy recalculation of deposited shower energy in atmosphere measured by fluorescence detectors by addition of estimated missing energy carried away by muons and neutrinos. The goal is to find the connection between the missing energy and the number of muons hitting the surface detectors. Better energy reconstuction methods will lower systhematic errors and can contribute to more educated physical interpretation of measured data.

In the first chapter 1 physical properties of a cosmic ray shower and parameters of the fluorescence detector as well as the reconstruction method used at the PAO will be discussed. Estimation of the shower missing energy using simulated data and its connection to number of shower muons will be shown in chapter two 2.2. Ultimately, in chapter three 3 the AugerPrime upgrade in connection to muon reconstruction method will be discussed.

Chapter 1

Cosmic ray shower

Direct detection and measurement of ultra-high energy primary cosmic ray particles is practically impossible due to their low impact flux on the atmosphere. However, the energy of a primary particle is transformed into the shower of secondary cosmic ray particles still energetic enough to create subsequent particles and to excite atmospheric molecules. Deexcitation of molecules in the form of UV light and impact of the shower front on the ground is registered by fluorescence and surface detectors respectively. The cosmic ray shower is then reconstructed using collected data from both detectors.

1.1 Shower composition

Primary cosmic ray particle such as proton or heavier nucleus undergoes hadronic reaction in upper atmosphere after traversing approximately 25-40 g.cm^{-2} in average. A spallation process of atmospheric nuclei with emission of protons, neutrons and nuclei fragments as well as creation of unstable pions and kaons can occur. Such particles form a hadronic part of the shower and at first several generations still have enough energy to create new particles with subsequent hadronic interactions. This multiplication of the hadronic part stops when the energy of unstable hadrons decrease under the critical energy when decay is more probable then hadronic interactions.

Decay of unstable charged pions and kaons give rise to a muonic part of the shower. Muons are unstable leptons with minimal interaction with atmosphere and therefore substantial part of signal from surface detectors is caused by relativistic muons reaching the ground. Since muons excite the atmosphere minimally they represent the first shower part carrying away the missing energy from detectors.

The most interacting part of the shower is an electromagnetic component which arises mainly from decays of neutral pions into photons and muons into electrons and neutrinos. Energetic photons can undergo a conversion process into electron and positron which can both subsequently emit new photons in the processes of bremsstrahlung. This electromagnetic cascade quicky amplifies the electromagnetic part of the shower which contributes to the major part of a fluorescence detector signal.

Finally, the last part of the shower consists of neutrinos emerged from various decay reactions. Neutrinos together with muons also carry away substantial part of the shower energy as they practically do not react with atmosphere or surface detectors. For a

schematic picture of the cosmic ray shower see Figure 1.1.

1.2 Shower developement

Simple semi-empirical Heitler's model of a shower developement [3] predicts roughly 10 charged and 5 neutral pions emerged in every hadronic cascade interaction with interaction lenght about 120 g.cm^{-2} in air until pions reach critical energy of 20 GeV. Although these values vary with energy they can be held as constants over pion energy range $10 - 1000$ GeV. Model predicts total number of interactions before reaching the critical energy as $3, 4, 5, 6$ for primary energies $10^{14}, 10^{15}, 10^{16}, 10^{17}$ eV with the list continuing in the same manner.

As for electromagnetic showers substantialy more cascade multiplications is predicted until the critical energy for electrons and positrons in air is reached because the radiation length of electrons and positrons in air is around 37 g.cm^{-2} and their critical energy in air is 85 MeV. Moreover, many electromagnetic subshowers is presented in shower for every neutral pion emerged in hadronic cascades.

At some moment in some slant depth X_{max} shower reaches its maximum size in the sum of all particles. This depth of shower maximum is one of significant measurable parametres of cosmic ray showers due to its connection to primary particle type and energy. From the Heitler's model accounting only for primary electromagnetic cascades and hadronic cascade one can derive important relation for proton induced showers

$$X_{max} = D \log_{10}(E_0), \quad D \approx 58 \text{ g.cm}^{-2}. \qquad (1.1)$$

The experimantaly measurable parameter D is called the elongation rate.

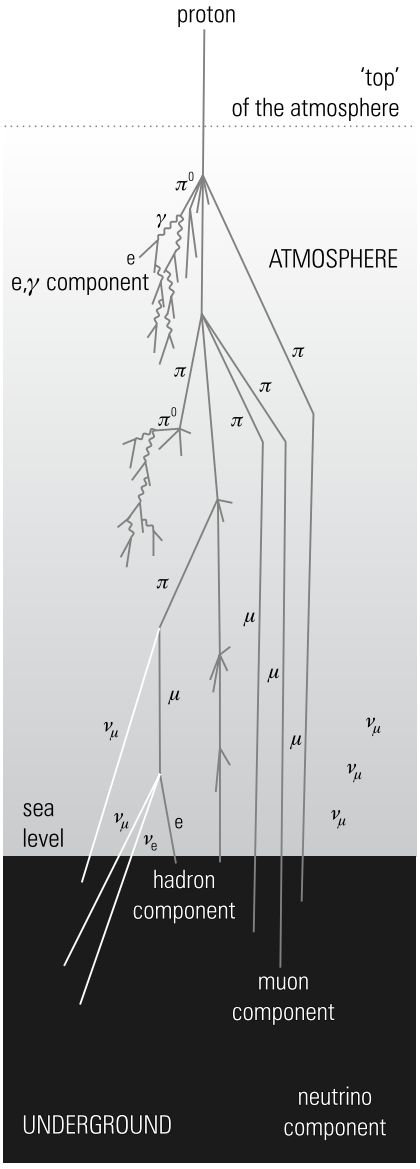

Figure 1.1: A model scheme of a cosmic ray shower composition. Taken from [2].

The particles maximum is followed by point in the slant depth where the shower energy deposition into atmosphere dE/dX is the largest. These two maxima are usually separated by a small slant depth of approximately 5 g.cm^{-2} while the latter is detectable by the fluorescence detectors as can be seen in Figure 1.2.

1.3 Shower detection

As was mentioned already two main types of detectors among others are used at the PAO. A surface detector array system and four stations with six air fluorescence detectors

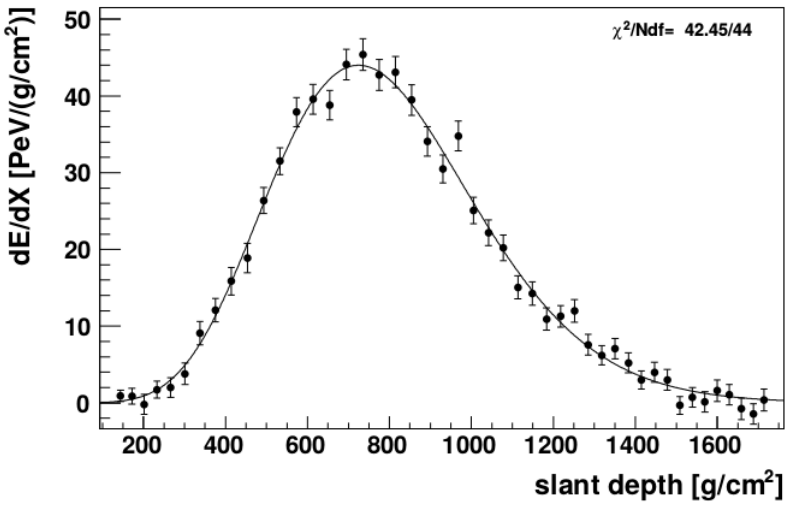

Figure 1.2: Measured shower energy deposit profile as a function of slant depth by the fluorescence telescope of the PAO. Data are fitted by the Gaisser-Hillas function. Taken from [4].

in each station overwatching the surface array. The fluorescence detectors measure UV light emitted from excited air molecules and require clear sky night without moon light contamination. This restriction somewhat limits the average observation time to only 13 % of the total time, whereas the surface detector array has unlimited observation time. Both detector systems are used in shower reconstruction and primary energy estimation. For the purpose of this paper only the fluorescence detector scheme will be briefly described.

1.3.1 Fluorescence detector of the PAO

Four fluorescence detector sites overwatch the surface detector array - Los Leones, Los Morados, Loma Amarilla and Coihueco. Each of four sites consists of six separated fluorescence telescopes with $30° \times 30°$ field of view resulting in the $180°$ coverage in azimuth. Fluorescence telescope scheme is depicted in Figure 1.3.

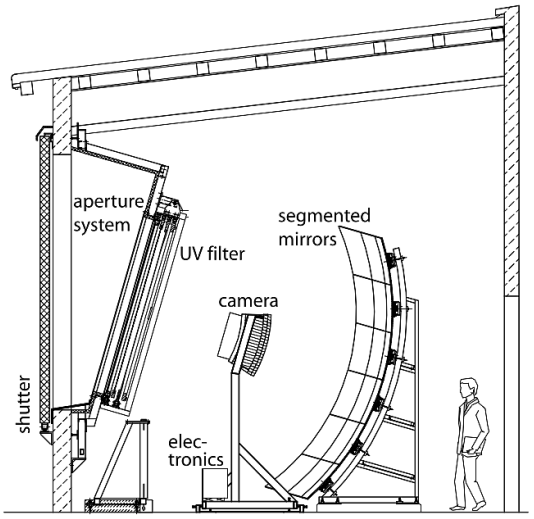

Figure 1.3: A scheme of the fluorescence telescope with main parts highlighted. Taken from [4].

The UV light emitted from nitrogen de-excitacion enters the fluorescence telescope through an optical filter transmitting only photons up to 410 nm in wavelength and thus eliminating the noise of any visible photons. Light is then transmitted through an aperture and a corrector ring onto a large segmented spherical mirror focusing the light on a 440 pixel camera. Every pixel represents a photomultiplier tube (PMT) capable of detecting even single photons. Light pulses in PMTs are being read every 100 ns and time order of activated PMTs enables the reconstuction of shower axis and

direction.

A telescope shutter is closed whenever the outside conditions do not enable measurement for example daylight, moonlight, rain or wind to protect the telescope.

1.4 Shower reconstruction

A sequence of activated fluorescence telescope pixels can be seen in Figure 1.4 with blue representing the first pixels being activated and red the last ones. From the knowledge of activated pixel positions a shower-detector plane (SDP) (Fig. 1.4) is experimantally fixed as the plane containing telescope position and shower axis.

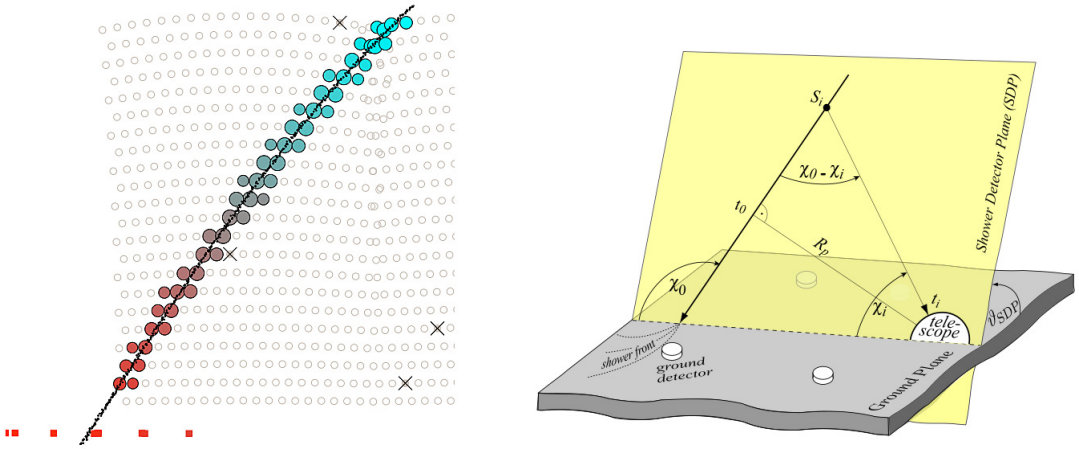

Figure 1.4: Left: A picture of the time progression of activated pixels in the fluorescence telescope by a cosmic ray shower with blue pixels being activated earlier than the red ones. Red squares represent activated surface detectors by the shower front. Right: A scheme of the shower-detector plane with depiction of important measured and fit parameters at a shower axis. Both pictures taken from [4].

Next, the time information of activated pixels is used to reconstruct the shower axis within the SDP. If the distance of closest approach of the shower axis to the telescope is R_p and shower front have crossed this point in time t_0, the time of i-th pixel activation can be represented by an equation

$$t_i = t_0 + \frac{R_p}{c} \operatorname{tg}\left(\frac{\chi_0 - \chi_i}{2}\right), \tag{1.2}$$

where c is the speed of light in vacuum, χ_0 is the angle between the shower axis and a ground plane in the SDP and χ_i is the angle between i-th activated pixel and the ground plane in the SDP. By fitting the eqation (1.2) to measured χ_i and t_i one can obtain the shower axis parameters R_p and χ_0.

Possible variety of fitted (R_p,χ_0) for a single shower can be resolved by utilising data from activated surface detectors which significantly lowers the total error of the shower reconstruction to 50 m in shower core location and 0.6° in shower arrival direction. This hybrid detector apporoach is very useful since the surface detectors duty cycle is 100% and majority of events above $10^{18.3}$ eV detected by the fluorescence detectors is accompanied by activation of several surface stations.

With shower geometry being reconstructed, next step is to estimate shower energy deposition into the atmosphere by measuring the light collected by the fluorescence telescopes. Careful measuring of atmosphere properties is needed to estimate light attenuation in the atmosphere while traversing from the shower to the telescope. Resulting plot of the shower energy deposition into the atmosphere is shown in Figure 1.2. It is fitted by the Gaisser-Hillas function (2.6) defined in chapter 2.2 and integrated to obtain the calorimetric energy deposited into the atmosphere.

Mentioned already, the computed value represents roughly 80-95% of the shower total energy. The rest of the shower energy - "invisible energy" - is carried away in the form or muons and neutrinos. The non-interacting shower fraction is estimated using Monte Carlo simulations for various primary particle parameters and will be disscused in the following chapter.

Chapter 2

Missing energy

Several methods for estimating the missing energy of the cosmic ray shower using Monte Carlo simulations were proposed. Current reconstruction method used at the PAO utilizes parametrization of the missing energy as a function of the calorimetric energy. Let us define, in accord with other papers [5, 6, 7], the quantity C_{miss} with a relation

$$C_{miss}(E_{cal}) = \frac{E_{cal}}{E_0}, \tag{2.1}$$

where E_{cal} is the calorimetric energy and E_0 the primary energy of a shower. Dividing a simple equation

$$E_{cal} = E_0 - E_{miss} \tag{2.2}$$

by E_0, with E_{miss} representing the missing energy of a shower, results into

$$C_{miss} = \frac{E_{cal}}{E_0} = 1 - \frac{E_{miss}}{E_0}. \tag{2.3}$$

Therefore, with knowledge of behavior of the quantity $C_{miss}(E_{cal})$ for different E_{cal}, one can simply obtain the shower primary energy from measured calorimetric energy as follows

$$E_0 = \frac{E_{cal}}{C_{miss}(E_{cal})}. \tag{2.4}$$

Because of shower-to-shower fluctuations of calculated E_{cal} for the same parameters of shower primary particles, one needs to consider parametrization of mean value $\langle C_{miss} \rangle$ as a function of measured E_{cal} during the shower reconstruction. A good parametrization is

$$\langle C_{miss} \rangle = \frac{\langle E_{cal} \rangle}{E_0} = a - b \left(\frac{\langle E_{cal} \rangle}{1\,\mathrm{EeV}} \right)^c, \tag{2.5}$$

where a, b and c are constants characterizing used hadronic interaction model.

2.1 Missing energy calculation

To calculate the missing energy part of a stimulated cosmic ray shower, a process similar to the one used in the shower energy reconstrucion was used. Normally, with the

knowledge of the shower longitudal profile, energy deposition $\mathrm{d}E/\mathrm{d}X(X)$ as a function of slant depth X is fitted according to the Gaiser-Hillas function in the following form

$$f_{GH}(X) = \left(\frac{\mathrm{d}E}{\mathrm{d}X}\right)_{max} \left(\frac{X - X_0}{X_{max} - X_0}\right)^{\frac{X_{max}-X_0}{\lambda}} e^{\frac{X_{max}-X}{\lambda}}. \tag{2.6}$$

Through this four-parameter fit the largest energy deposit $(\mathrm{d}E/\mathrm{d}X)_{max}$ as well as the slant depth of this maximum X_{max} is obtained. Two other parameters X_0 and λ represent the slant depth of first interaction and radiation lenght respectively. With the function (2.6) obtained, its integration by slant depth reveals the shower calorimetric energy

$$E_{cal} = \int_0^\infty f_{GH}(X)\mathrm{d}X. \tag{2.7}$$

Numerical integration of simulated shower data is one way to obtain the results needed. However, an analytical form of the integral (2.7) exists in the following form

$$E_{cal} = \lambda \left(\frac{\mathrm{d}E}{\mathrm{d}X}\right)_{max} \left(\frac{e\lambda}{X_{max} - X_0}\right)^{\frac{X_{max}-X_0}{\lambda}} \Gamma\left(\frac{X_{max} - X_0}{\lambda} + 1\right), \tag{2.8}$$

where Γ represents the Gamma function. By inserting parameter $(\mathrm{d}E/\mathrm{d}X)_{max}$ from (2.8) into (2.6) we obtain

$$f_{GH}(X) = \frac{E_{cal}}{\lambda} \left(\frac{X - X_0}{\lambda}\right)^{\frac{X_{max}-X_0}{\lambda}} e^{\frac{X_0-X}{\lambda}} \left[\Gamma\left(\frac{X_{max} - X_0}{\lambda} + 1\right)\right]^{-1}. \tag{2.9}$$

Hence, new fitting relation was obtained with E_{cal} becoming one of the fit parameters so that the shower calorimetric energy can be directly calculated by fitting equation (2.9) to the shower longitudal profile. The fitting itself remains four-parametrical in E_{cal}, X_{max}, X_0 and λ.

With E_{cal} computed and with the knowledge of the shower primary energy E_0, being one of the simulation primary parameters, equation (2.2) resp. (2.3) is used to obtain E_{miss} resp. C_{miss} for a processed shower.

2.2 Data simulation and processing

Cosmic ray showers were simulated by program CONEX [8] that combines Monte Carlo simulations and numerical evaluation of cascade equations to obtain fast 1D shower data. Two of the newest hadronic interaction models were used - EPOS LHC and QGSJET-II-04. Seven primary energy groups with values of $\log E_0$ [eV] - 17, 17.5, 18, 18.5, 19, 19.5, 20 - and two primary particle types - proton and iron nucleus - were included. For every possible combination of previously listed initial parameters and interaction models 200 showers were simulated with total number or simulations reaching 5600. A shower zenith angle was held at 60° for every simulated shower to obtain a long profile in X.

For every simulated shower two step fitting procedure was realized. First, the simulated shower energy deposit profile was fitted to equation (2.6) to estimate the parameters X_{max}, X_0 and λ. Then a second data fit was performed to equation (2.9) while utilizing the parameters estimated in the previous fit and additionally the parameter E_{cal}. An

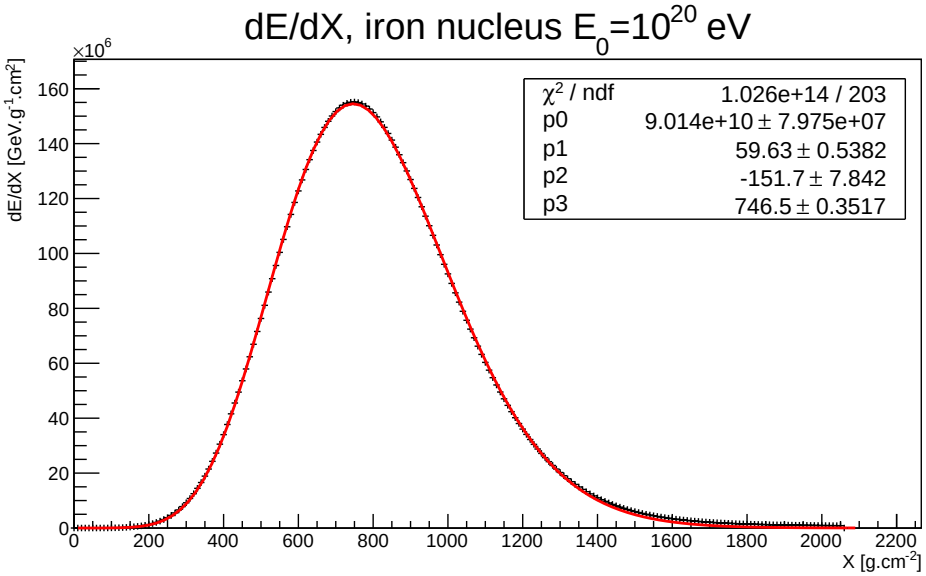

Figure 2.1: A fitted longitudal energy profile of a 10^{20} eV iron nucleus induced shower. Parameters from $p0$ to $p3$ represent E_{cal}, λ, X_0 and X_{max} in this order.

example of the fitted plot of simulated shower energy deposit profile of a 10^{20} iron induced shower is shown in Figure 2.1.

By estimation of average E_{miss} for all showers with specific primary energy and primary particle type, the behavior of missing to primary energy ratio - $\langle E_{miss}\rangle/E_0$ - was revealed. In Figure 2.2 histograms of evaluated E_{miss}/E_0 ratios for proton and iron induced showers with primary energy $E_0 = 10^{17}$ eV are shown for both hadronic interaction models. Histograms corresponding to other primary energies are presented in Appendix A. With increase in primary energy the average $\langle E_{miss}\rangle/E_0$ ratio decreases as can be seen in Figure 2.3. The results from both interaction models are comparable, albeit higher by cca 1-2 % for QGSJET-II-04. The highest portion of missing energy is predicted for iron induced showers reaching up to 21 % for $E_0 = 10^{17}$ and falling to 10 % for $E_0 = 10^{20}$ eV. Smaller missing energy portion is predicted for proton induced showers with maximum at 14 % and minimum at 7 % for the same energies.

Furthermore, the parametrization for $\langle C_{miss}\rangle$ was estimated by fitting equation (2.5) to simulated data. The results for the parametrization constants a, b and c are listed in Table 2.1 toghether with results from [7] utilizing older hadronic interaction models. Parametrization curves as functions of E_{cal} for different interaction models are compared in Figure 2.4. All interaction models predict similar behavior of C_{miss} with increasing E_{cal}. The smallest C_{miss} values for all E_{cal} are predicted by QGSJET-II-04 and then by EPOS LHC, whereas the largest values are predicted by SYBILL.

Final set of parameters a, b and c used in the shower energy reconstruction would then be calculated as an average over both interaction models with estimating the primary particle dependance as an equal mixture of protons and iron nuclei results. Such computed results are shown in Table 2.2 and compared to the previous results from [7] and [5].

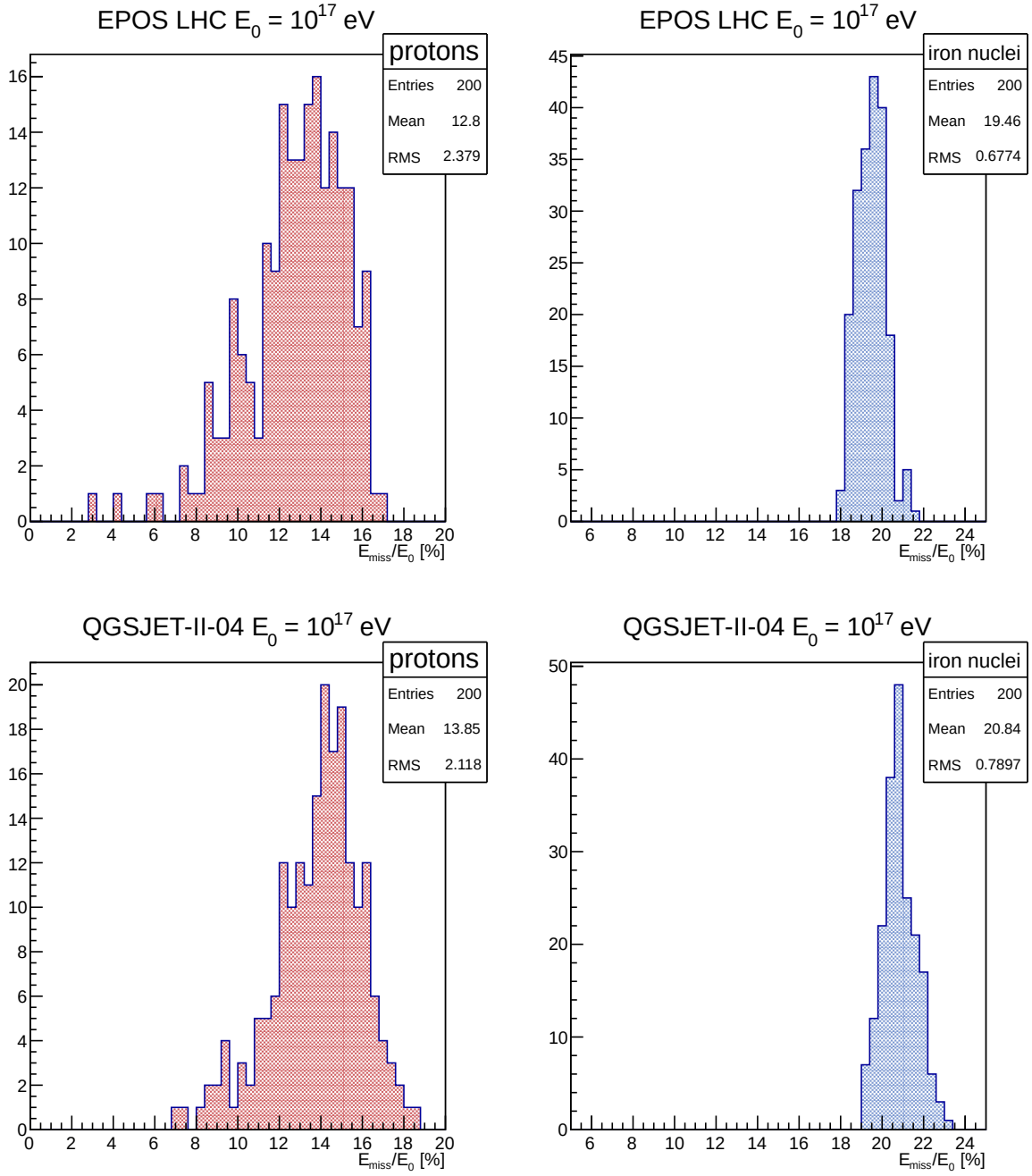

Figure 2.2: Histograms of evaluated E_{miss}/E_0 ratios for all simulated showers with primary energy $E_0 = 10^{17}$ eV for both primary particle types and both interaction models.

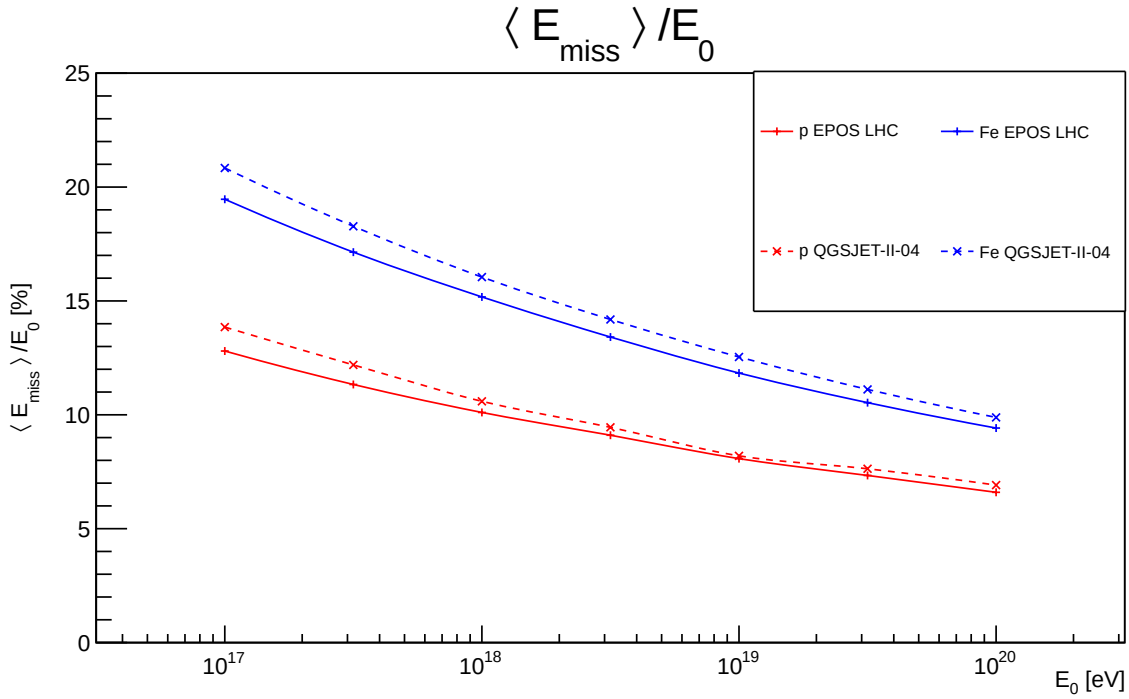

Figure 2.3: The behavior of $\langle E_{miss} \rangle / E_0$ ratio for different primary energies and particle types shows decrease in missing energy portion with increasing E_0.

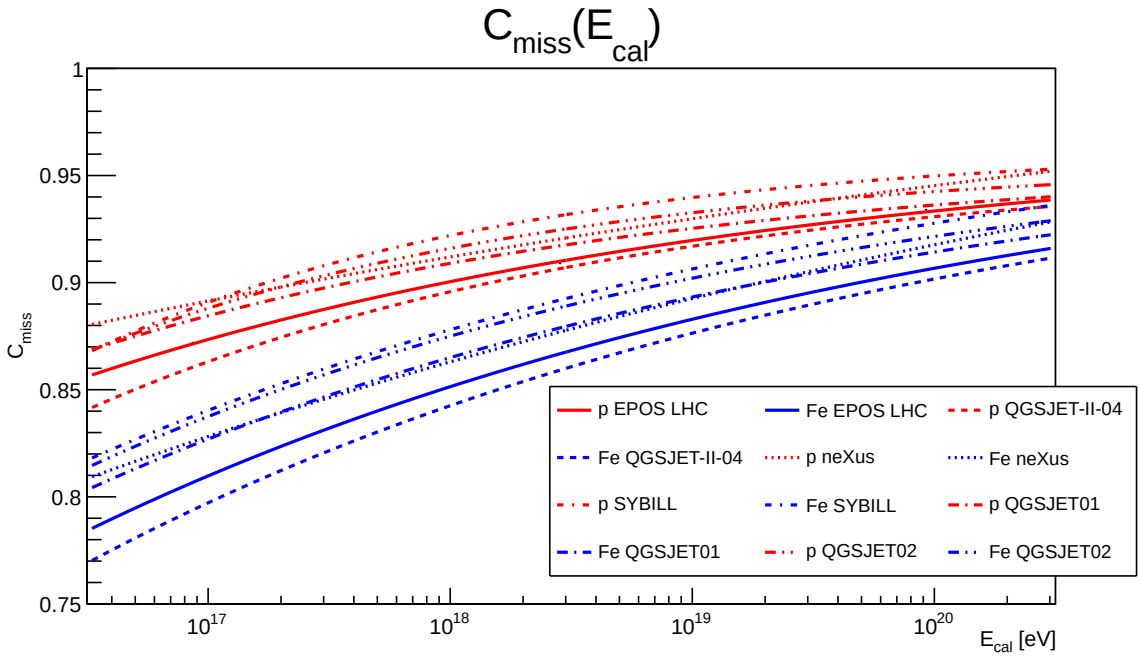

Figure 2.4: Parametrization curves of E_{cal}/E_0 as functions of E_{cal} predicted by different hadronic interaction models.

Table 2.1: Values of the parametrization constants for different hadronic interaction models. Results from this work are in bold, other are taken from [7].

	protons		
	a	b	c
EPOS LHC	$\mathbf{0.968 \pm 0.005}$	$\mathbf{0.067 \pm 0.005}$	$\mathbf{-0.147 \pm 0.011}$
QGSJET-II-04	$\mathbf{0.956 \pm 0.004}$	$\mathbf{0.060 \pm 0.004}$	$\mathbf{-0.187 \pm 0.012}$
neXus	1.046	0.134	-0.062
SYBILL	0.963	0.041	-0.246
QGSJET01	0.958	0.049	-0.176
QGSJET02	0.957	0.041	-0.226

	iron nuclei		
	a	b	c
EPOS LHC	$\mathbf{0.980 \pm 0.003}$	$\mathbf{0.129 \pm 0.003}$	$\mathbf{-0.121 \pm 0.003}$
QGSJET-II-04	$\mathbf{0.976 \pm 0.002}$	$\mathbf{0.133 \pm 0.002}$	$\mathbf{-0.127 \pm 0.002}$
neXus	1.059	0.196	-0.071
SYBILL	0.993	0.115	-0.123
QGSJET01	0.975	0.110	-0.129
QGSJET02	0.972	0.097	-0.142

Table 2.2: Final values of the parameters a, b and c. Values in bold are results of this work, whereas the others are showed for comparison. Second line results are taken from [7], third line results are taken from [5].

a	b	c
$\mathbf{0.970 \pm 0.004}$	$\mathbf{0.097 \pm 0.004}$	$\mathbf{-0.146 \pm 0.007}$
0.978	0.085	-0.135
0.967	0.078	-0.140

2.3 Missing energy estimation through shower muon measurement

While the C_{miss} method is currently employed in the shower energy reconstruction process at the PAO, a more precise method connectig missing energy with a shower muon part is known [6]. Muons originating in atmosphere during shower propagation constitute the major part of shower undetected particles thus a direct link between the shower missing energy E_{miss} and the number of muons reaching Earth's ground N_μ is expected. All 5600 simulated showers from section 2.2 were evaluated to obtain the plot in Figure 2.5 showing logarithm of E_{miss} as a function of logarithm of respecive N_μ with approximatively linear dependance. A linear fit was applied to the plot with a result

$$\log_{10}(\tfrac{E_{miss}}{1\,\mathrm{eV}}) = a.\log_{10}(N_\mu) + b \tag{2.10}$$

$$a = 0.9656 \pm 0.0007 \tag{2.11}$$

$$b = 10.822 \pm 0.005. \tag{2.12}$$

Hence, the shower missing energy can be estimated solely from measured shower muons reaching the ground using the relation (2.10). This reconstruction method is completly independent of the shower calorimetrical energy and it is estimated without dependance

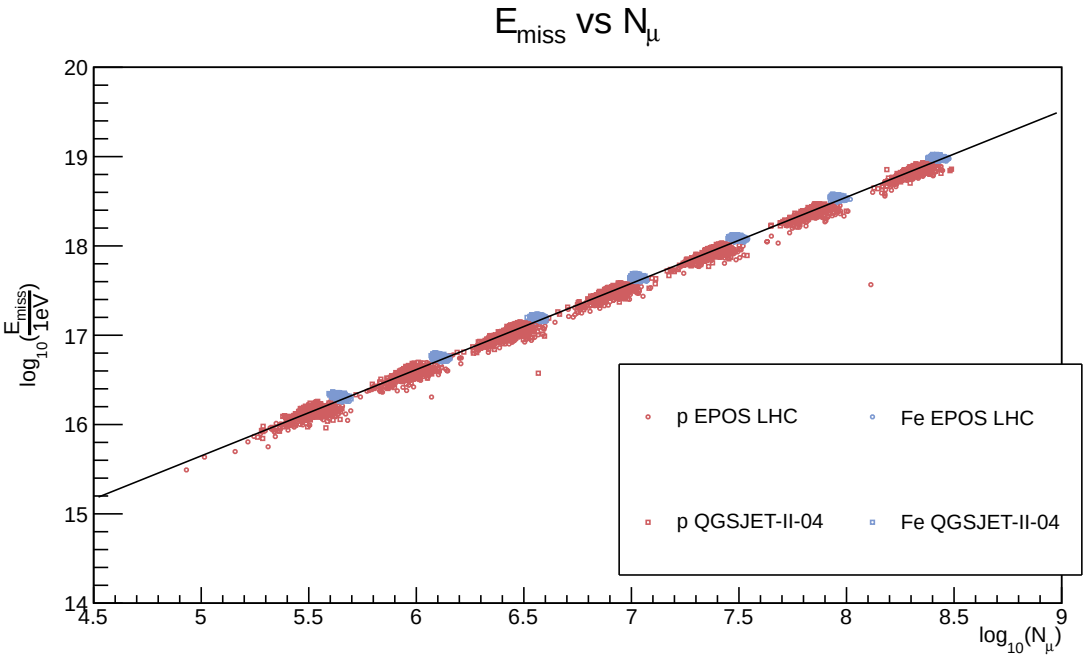

Figure 2.5: A fitted graph showing relation between logarithm of missing energy of a shower and logarithm of the shower muon count.

on simulated shower primary particles or used interaction models. Thus the precission of muon reconstruction method will be significantly better than the C_{miss} method as can be seen in the comparison of relative energy reconstruction errors between the C_{miss} method and the method utilizing muons in Figure 2.6.

Naturally, taking the final parameters of the C_{miss} parametrization as an even mixture of simulated proton and iron nucleus primaries results into fact, that reconstructed shower missing energy would be overestimated for lighter primary particles resp. underestimated for heavier primaries relatively to the average between proton and iron mass number. This effect is clearly visible in Figure 2.6. On the contrary, the muon reconstruction method error rises merely from the fitting in Figure 2.5, where the fitted line goes slightly under the iron induced shower bulks resp. above the proton induced shower bulks. Overall, a decrease of the histogram RMS of reconstructed energy errors values for muon method can be seen.

On the other hand, insufficient estimation of total shower muon count at the PAO prevents the muon reconstruction method from being succesfully applied in the process of shower energy reconstruction. The observatory upgrade currently underway - the Auger-Prime - should eventually make the precise muon component measurement possible.

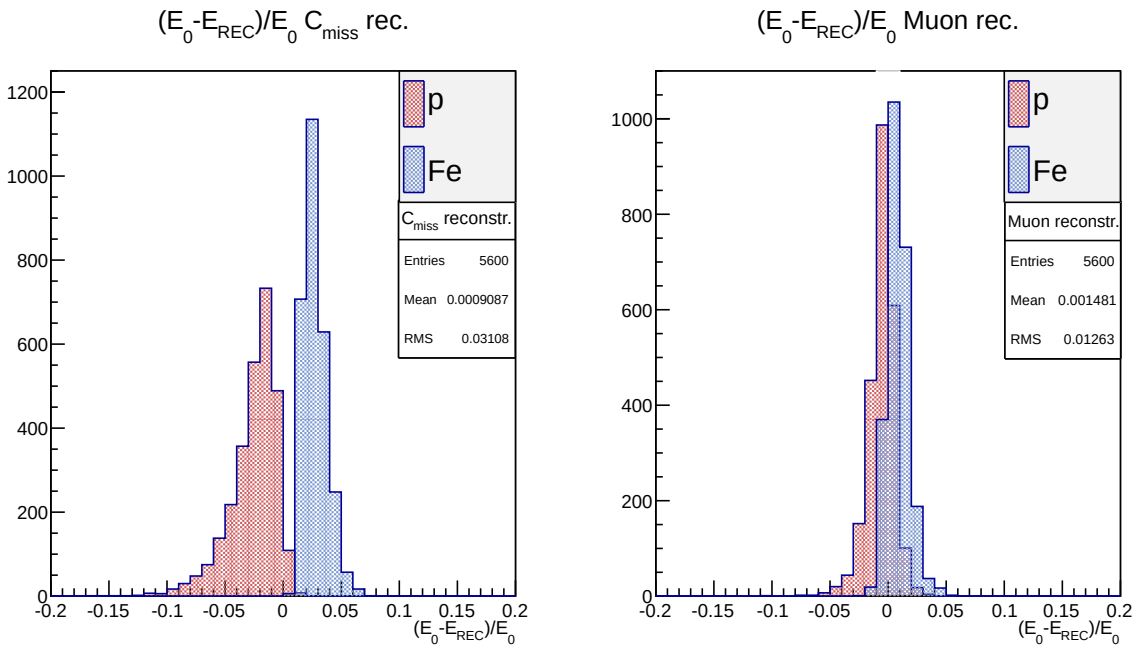

Figure 2.6: Comparison of the relative errors between reconstructed E_{REC} and simulated E_0 shower primary energies when utilizing the C_{miss} (left) and the muon (right) reconstruction method. All simulated showers by both interaction models were reconstructed by both methods. The muon reconstruction method shows nearly three times narrower distribution of $(E_0 - E_{REC})/E_0$.

Chapter 3

The AugerPrime upgrade

The AugerPrime upgrade is currently (2017) at the phase of deployment of new detectors with scheduled completion in year 2018 [9]. The upgrade consists mainly of newly deployed plastic surface scintillator detectors (SSD) on the top of each of the 1660 SD stations, installation of underground muon detector (UMD) in the infill area of a denser SD array and an upgrade of FD telescopes to extend the current operational duty cycle by 50 %.

With upgraded observatory, obtaining of high-quality data with a new composition-sensitive information for every event is anticipated. This will help not only with the primary particle identification and energy reconstruction at the high energy range above the ankle but will also help to reduce systematic uncertainties related to modeling of hadronic showers. Generally, a new insight into the cosmic ray flux suppresion area at the highest energies is expected.

3.1 The surface detector upgrade

The SD array at the PAO consists of 1660 water Cherenkov stations (WCS) arranged into triangular grid with 1500 m spacing between stations covering overall more than 3000 km^2. Relativistic particles passing through station's water create Cherenkov light which is collected by three photomultiplier tubes. An upgrade for the WCS electronics and PMT signal readout is currently underway to improve station dynamic range and to decrease the amount of saturated PMT signals in the stations near shower core.

Main upgrade is the deployment of 4 m^2 plastic scintillators. The SSD unit consists of two modules each integrally read out by wavelenght shifting cables conducting light to one photo-detector. A model of the upgraded station with SSD on the top can be seen in Figure 3.1.

With the SSD being more sensitive to the electromagnetic part than the WCS which is sensitive to the sum of muonic and electromagnetic component, signal from both detector types can be compared to estimate shower muon component more precisely. Thus the muon reconstruction method can be utilized to improve shower energy determination.

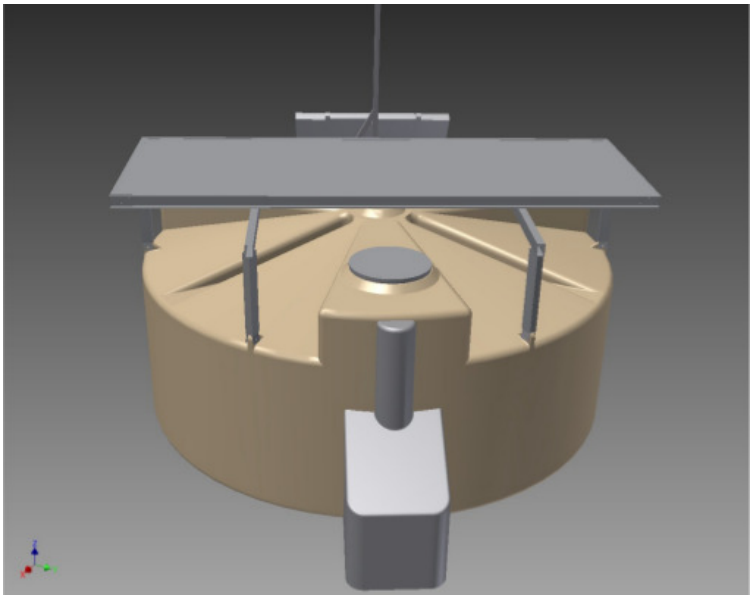

Figure 3.1: A model of SD station with water tank and scintillator on the top. Taken from [9].

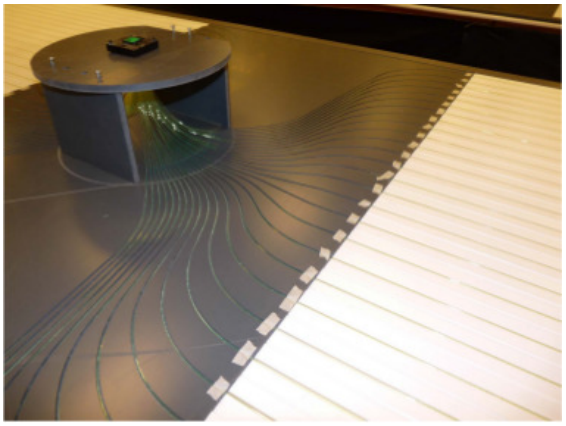

Figure 3.2: A figure of an AMIGA prototype consisting of 32 plastic scintillator bands on each side. Taken from [9].

3.2 The underground muon detector

Another detector being deployed at the PAO to strenghten the shower muon part measurement is the underground muon detector. The UMD will act as fine-tuning for the muon measurement by the WCS and SSD stations and will span under the SD infill area of 23.5 km^2. Each station of the UMD is comprised of a AMIGA muon counter system of 64 plastic scintillators with overall area of 30m^2 buried at the SD side at a depth of approximately 1.3 m to shield shower residual electromagnetic part.

The UMD will be effectively an extension of 7 AMIGA muon detectors stations currently at operation to 61 in total. A picture of an AMIGA prototype assembly is displayed in Figure 3.2.

Conclusion

In this research project high energy cosmic ray shower composition, developement and detection method at the Pierre Auger Observatory were studied. Main focus was on the estimation of a shower missing energy carried away by muons and neutrinos. Knowledge of the shower missing energy is needed for the succesful shower reconstruction process.

Two distinct methods for the missing energy calculation were elaborated. First one currently used at the PAO utilizes average values of calculated missing energies for simulated shower profiles of different energies and primary particles. In this work showers were simulated using hadronic interaction models EPOS LHC and QGSJET-II-04. Simulated data were analyzed and the C_{miss} parametrization of average missing energy as a function of calorimetric energy was estimated. Values of the C_{miss} parametrization parameters a, b and c were calculated and compared with previous results.

Second method uses a direct relation between the number of shower muons and the shower missing energy. The data set was fitted to obtain an equation relating the shower missing energy and the number of measured shower muons.

Both methods were compared using the simulated data. The muon reconstrucion method was found to be more precise, however current muon detection at the PAO is not sufficient enough to succesfully apply the method shower by shower.

Ultimately, the AugerPrime upgrade of the observatory and its potential in muon measurement was briefly discussed. Deployment of new scintillator detectors both above and under the surface detectors should substantialy increase the observatory shower reconstruction potential and elucidate the main cosmic ray puzzles at the highest energies.

Bibliography

[1] A. Aab et al. The Pierre Auger Cosmic Ray Observatory. *Nucl. Instrum. Meth.*, A798:172–213, 2015.

[2] C. Grupen. *Astroparticle physics*. Springer Science & Business Media, 2005, ISBN 978-3-540-25312-9.

[3] J. Matthews. A Heitler model of extensive air showers. *Astropart. Phys.*, 22:387–397, 2005.

[4] J. Abraham et al. The Fluorescence Detector of the Pierre Auger Observatory. *Nucl. Instrum. Meth.*, A620:227–251, 2010.

[5] Henrique M. J. Barbosa, F. Catalani, J. A. Chinellato, and Carola Dobrigkeit. Determination of the calorimetric energy in extensive air showers. *Astropart. Phys.*, 22:159–166, 2004.

[6] M. Nyklíček and P. Trávníček. On the size of missing energy of cosmic ray showers. *Proceedings of the 31st ICRC Lodz*, paper 0240, 2010.

[7] M. Nyklíček, J. Řídký, and P. Trávníček. Influence of hadronic interaction models on determination of chemical composition and size of the missing energy. *GAP notes*, 2008.

[8] T. Bergmann et al. One-dimensional hybrid approach to extensive air shower simulation. *Astropart. Phys.*, 26:420–432, 2007.

[9] Alexander Aab et al. The Pierre Auger Observatory Upgrade - Preliminary Design Report, 2016, available at: *https://arxiv.org/abs/1604.03637*.

Appendix A

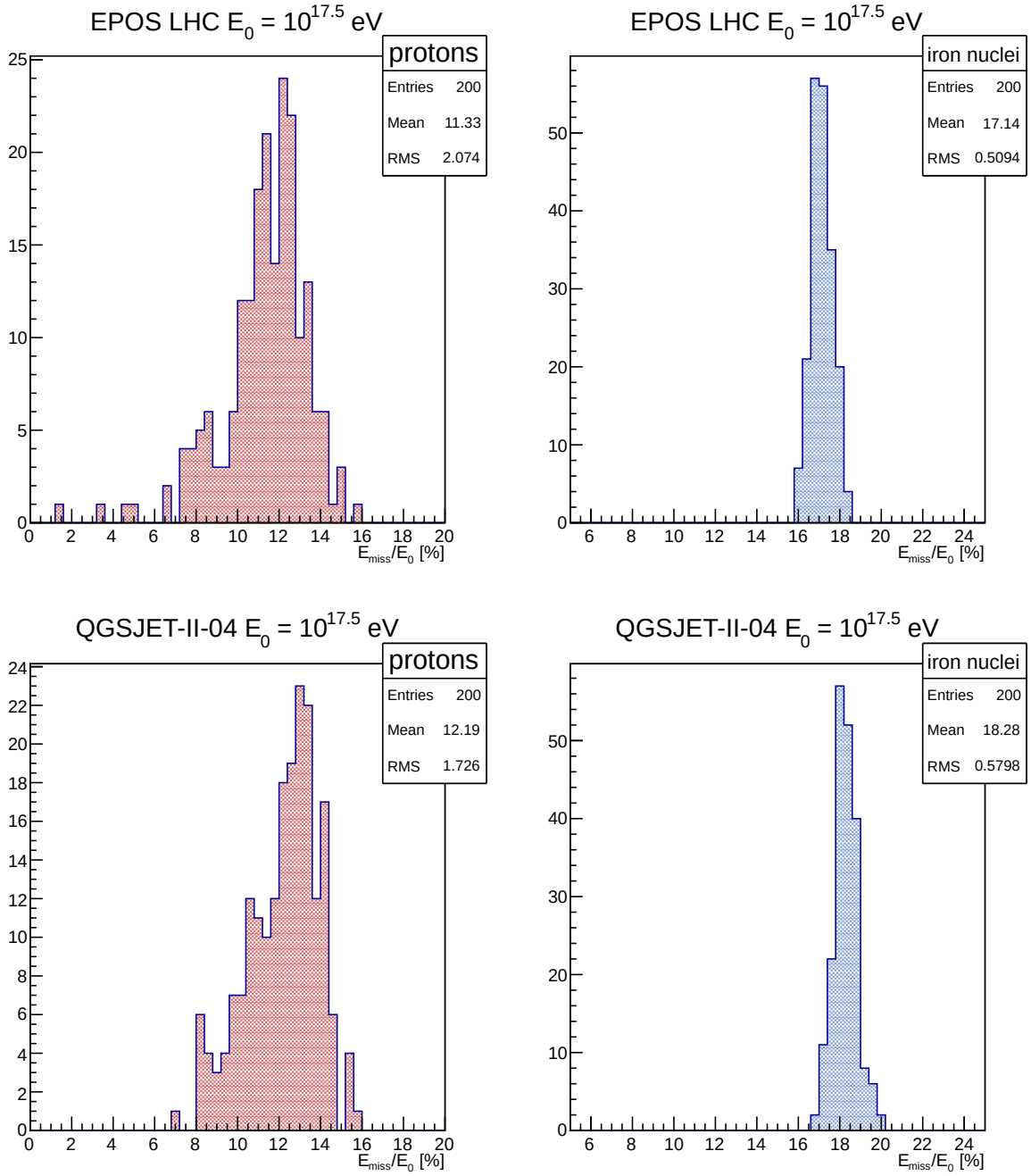

Figure 3.3: Histograms of evaluated E_{miss}/E_0 ratios for all simulated showers with primary energy $E_0 = 10^{17.5}$ eV for both primary particle types and both interaction models.

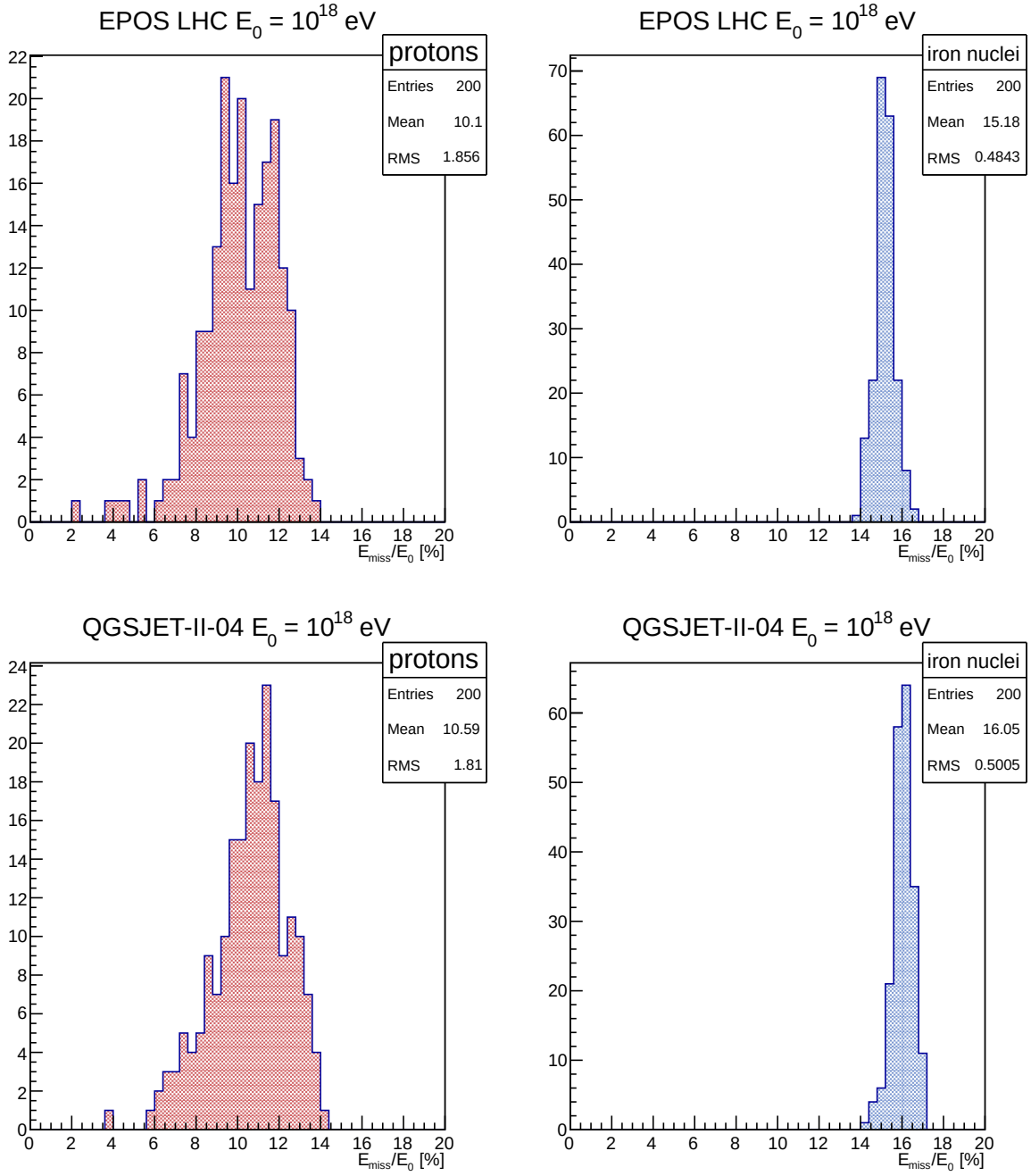

Figure 3.4: Histograms of evaluated E_{miss}/E_0 ratios for all simulated showers with primary energy $E_0 = 10^{18}$ eV for both primary particle types and both interaction models.

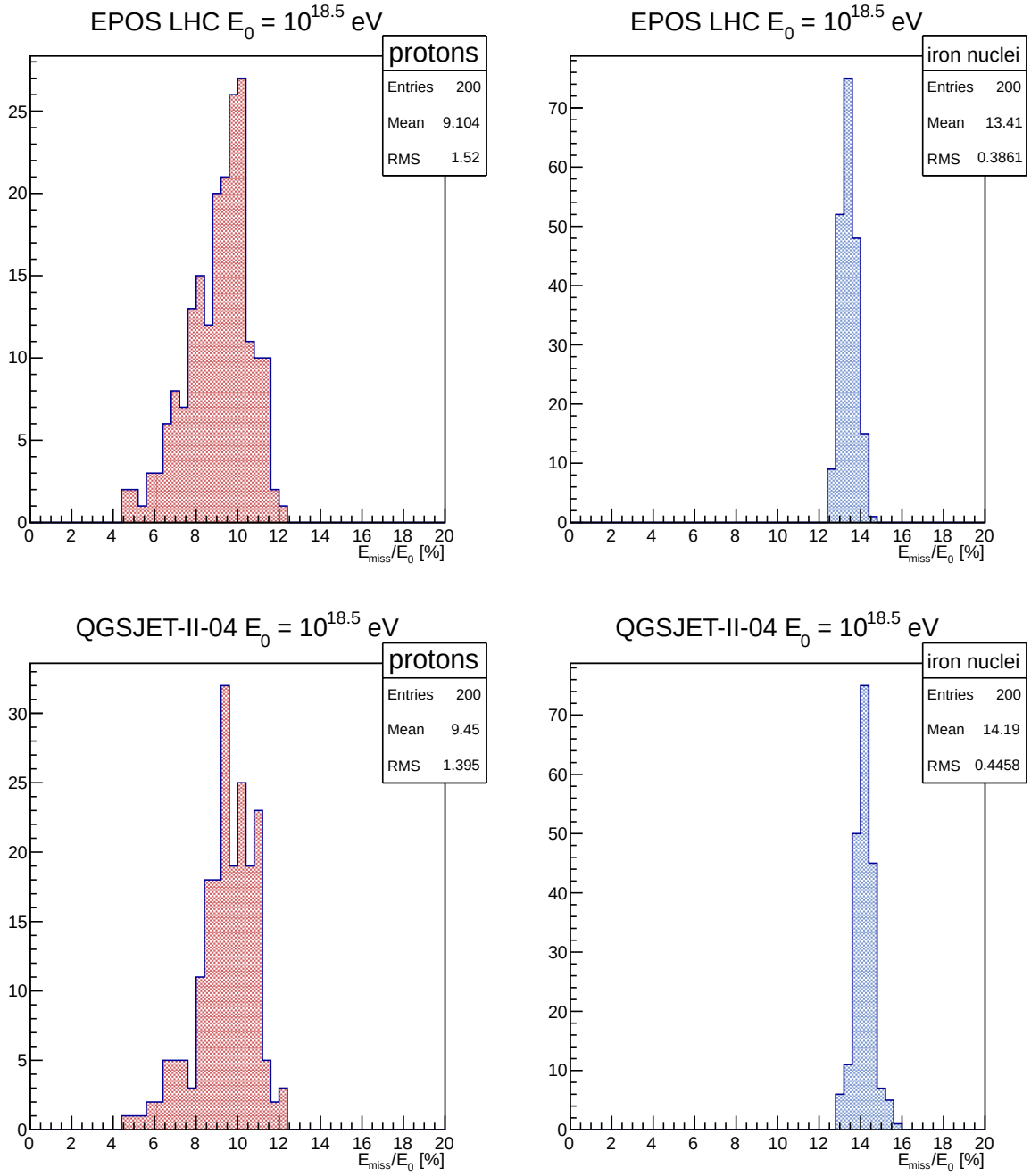

Figure 3.5: Histograms of evaluated E_{miss}/E_0 ratios for all simulated showers with primary energy $E_0 = 10^{18.5}$ eV for both primary particle types and both interaction models.

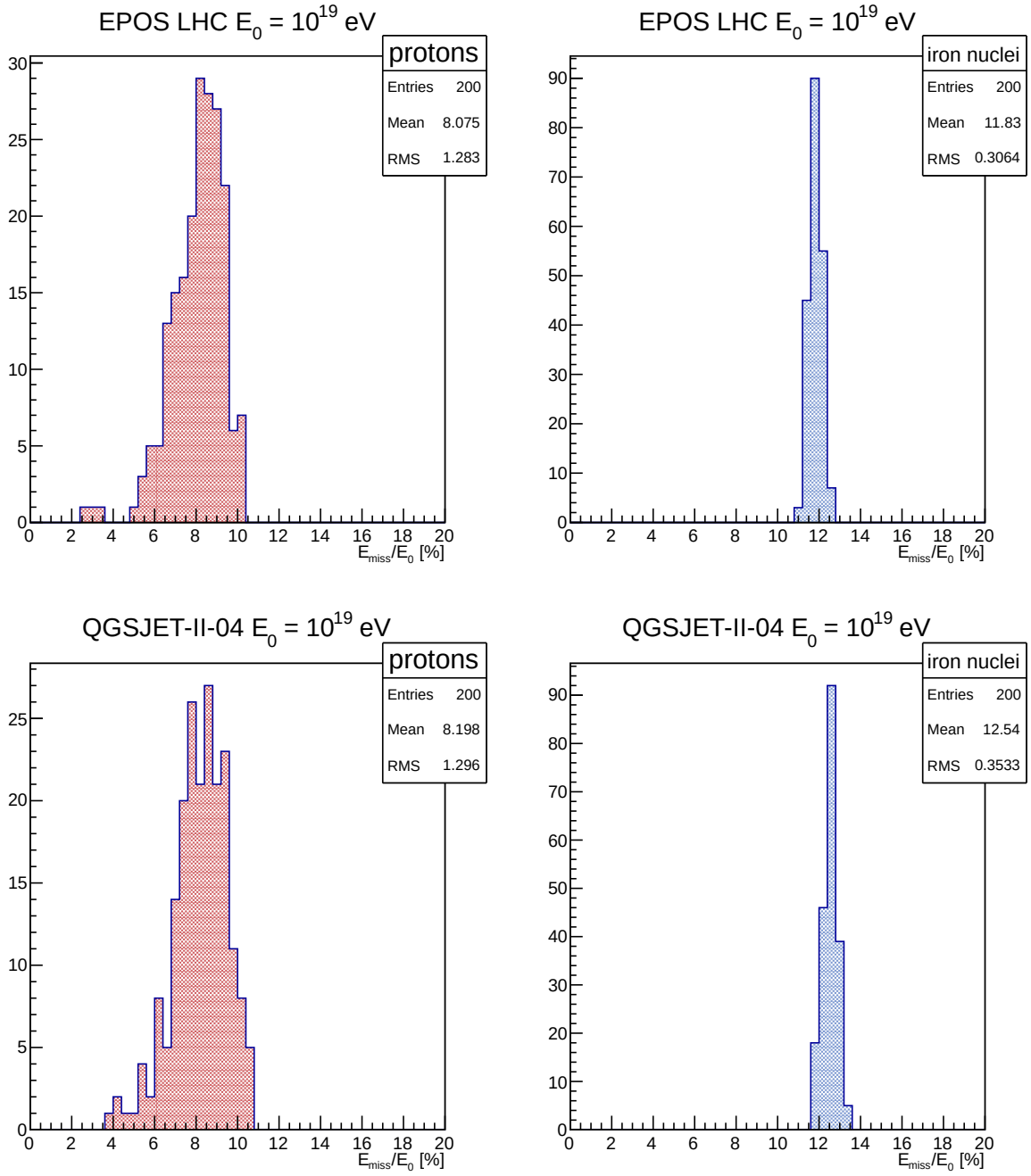

Figure 3.6: Histograms of evaluated E_{miss}/E_0 ratios for all simulated showers with primary energy $E_0 = 10^{19}$ eV for both primary particle types and both interaction models.

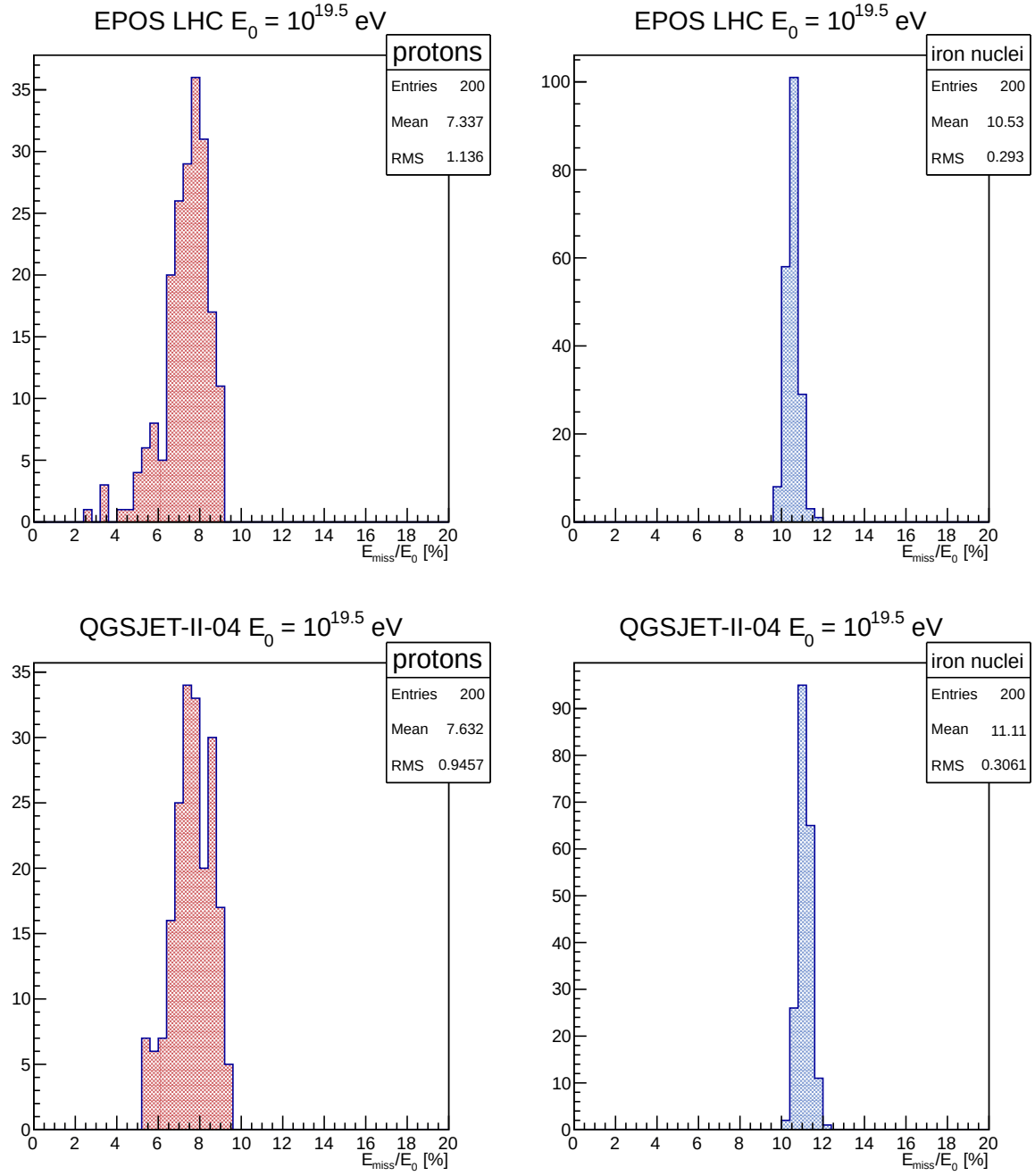

Figure 3.7: Histograms of evaluated E_{miss}/E_0 ratios for all simulated showers with primary energy $E_0 = 10^{19.5}$ eV for both primary particle types and both interaction models.

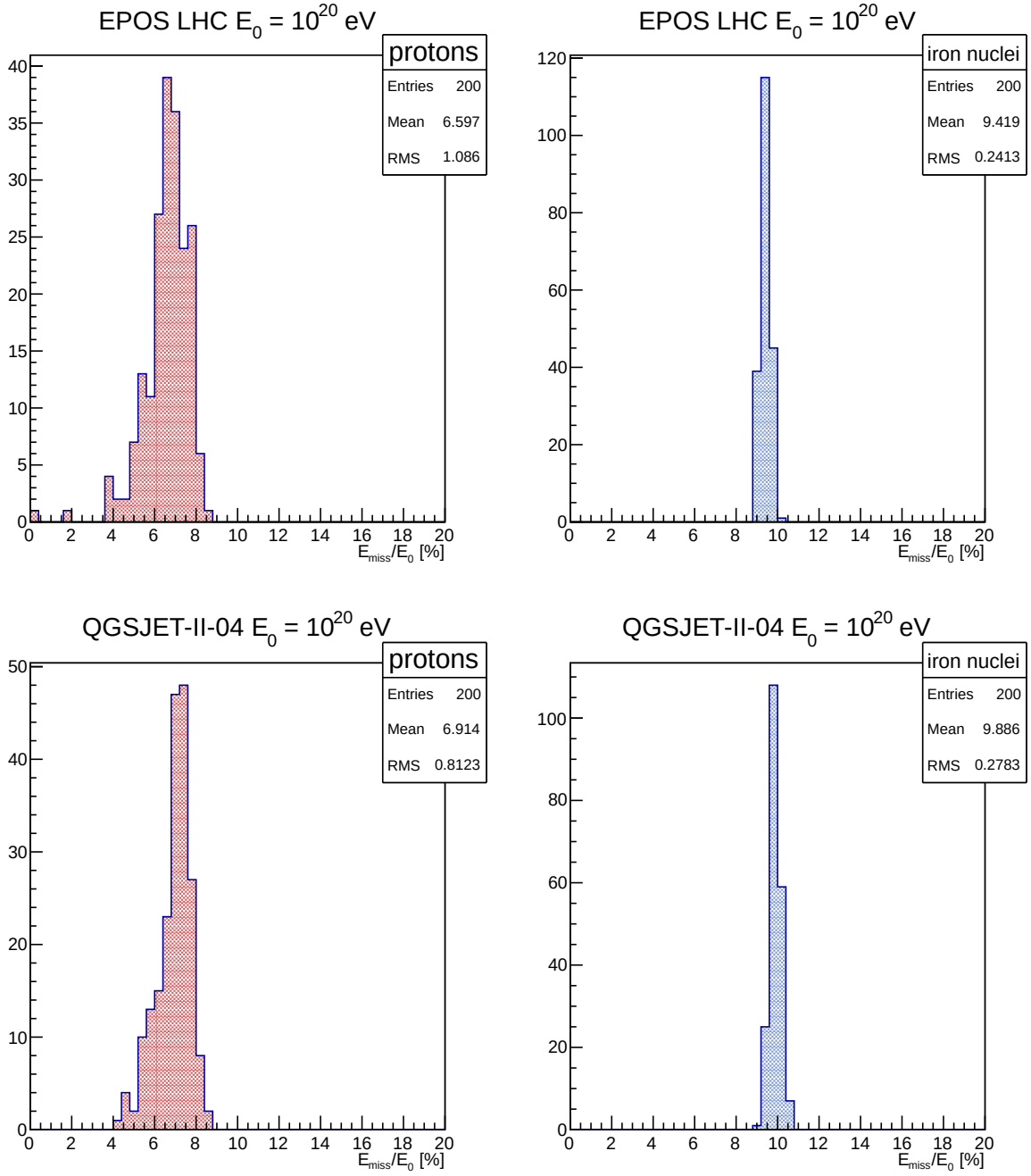

Figure 3.8: Histograms of evaluated E_{miss}/E_0 ratios for all simulated showers with primary energy $E_0 = 10^{20}$ eV for both primary particle types and both interaction models.